Available online at www.sciencedirect.com
ScienceDirect
International Journal of Heat and Mass Transfer 50 (2007) 1953–1962
International Journal of HEAT and MASS TRANSFER
www.elsevier.com/locate/ijhmt

Local heat transfer coefficients in spray cooling systems measured with temperature oscillation IR thermography

S. Freund [a], A.G. Pautsch [b], T.A. Shedd [b,*], S. Kabelac [a]

[a] Institute for Thermodynamics, Helmut-Schmidt-University of the Federal Armed Forces, D-22039 Hamburg, Germany
[b] Department of Mechanical Engineering, Multiphase Flow Visualization and Analysis Laboratory, University of Wisconsin–Madison, 1500 Engineering Drive, Madison, WI 53706-1609, USA

Received 24 March 2006; received in revised form 29 September 2006
Available online 12 December 2006

Abstract

This paper describes the application of the temperature oscillation IR thermography method to a spray cooling system in order to measure the spatial distribution of the heat transfer coefficients with a resolution of 0.4 mm. This technique allows for the rapid and fluid-independent evaluation of the heat transfer coefficient at the back side of a heat-transferring wall, relying on radiant heating, infrared temperature measurements, and a finite difference model of the wall. The results reveal the distribution of the local heat transfer coefficients over a surface cooled by a single- and a four-nozzle array of a multi-chip spray cooling module. The area averaged results from this method were compared to previous data measured using a conventional approach with a thermal test die and were found to be in good agreement.

Keywords: Spray cooling; Local heat transfer coefficient; Temperature oscillations

1. Introduction

As technology progresses, the power densities of electronic packages have continued to rise beyond the limits of conventional cooling. More sophisticated techniques to remove heat from the devices have been implemented, but many of these require a thermal interface material that adds a substantial amount of thermal resistance at high heat loads. Spray cooling is one method of direct liquid cooling that eliminates the need for a thermal interface material. When an inert fluid such as perfluorohexane (Fluorinert™ FC-72) is used, there is no risk to the electronic device from electrical arc or hydrogen diffusion. This direct cooling approach reduces the thermal resistance and leads to lower surface temperatures compared to any indirect system such as cold plates. Other benefits of spray cooling include improved thermal management, dense system packaging, and reduced weight of high heat flux computer chips, power electronics, and laser diode arrays.

1.1. Heat transfer coefficient measurement

The performance of conical sprays has been characterized by several research groups [1–3]. As an example, Cotler et al. reported a heat flux of up to 162 W cm^{-2} using a spray cooling system for an RF power amplifier with water as the working fluid [4]. There have also been numerous numerical simulations designed to model the interactions of droplets on a superheated surface and the corresponding heat transfer coefficients. Croce et al. have successfully modeled heat extraction from a surface by evaporation of impinging droplets [5]. Lee et al. have also modeled droplet interaction with a superheated surface and report heat transfer coefficients of between 0.1 and 2.0 W cm^{-2} K^{-1} in their simulations of an engine cylinder [6].

The two most commonly reported performance metrics for spray cooling systems are the critical heat flux (CHF)

* Corresponding author. Fax: +1 608 262 8464.
E-mail address: shedd@engr.wisc.edu (T.A. Shedd).

0017-9310/$ - see front matter © 2006 Elsevier Ltd. All rights reserved.
doi:10.1016/j.ijheatmasstransfer.2006.09.028

Nomenclature

c	wall heat capacity (J kg^{-1} K^{-1})	α	thermal diffusivity (m^2 s^{-1})
h	heat transfer coefficient (W cm^{-2} K^{-1})	δ	wall thickness (m)
i	number of images (–)	ω	angular frequency (rad s^{-1})
k	wall thermal conductivity (W m^{-1} K^{-1})	ϕ	phase delay (rad)
q''	heat flux (W cm^{-2})	ψ	dimensionless heat transfer coefficient (–)
T	temperature (°C)	ρ	wall density (kg m^{-3})
V''	volumetric droplet flux (ml s^{-1} cm^{-2})	ξ	dimensionless thickness (–)

and the heat transfer coefficient (h). The CHF is an upper limit on the power level that can be removed from a system while the heat transfer coefficient dictates the device temperature for a given heat load. Traditionally, the spray cooling heat transfer coefficient has been defined according to

$$\overline{h_{\mathrm{m}}} = \frac{q''}{(T_{\mathrm{surface}} - T_{\mathrm{inlet}})} \tag{1}$$

where q'' is the applied heat flux, T_{surface} is the temperature at the device surface, and T_{inlet} is the fluid temperature at the inlet of the spray nozzle. The bar over the h_{m} signifies a time-average while the subscript m specifies that h is a spatial average. The heat flux is typically assumed to be uniform over the surface and T_{surface} is measured at discrete locations on the device. The surface temperature is typically measured in two ways, depending on the heating element. If cartridge heaters in a copper block are used, then multiple thermocouples placed along the conduction path are used to extrapolate the temperature to the surface.

This single temperature measurement is typically obtained at the center of the heater, which in most cases is located directly under the center of the spray where the heat transfer coefficient is the largest. This may lead to a reported heat transfer coefficient that is substantially higher than the average surface heat transfer coefficient; further study is needed, however, to support this assertion. When thermal test dies are used, the junction temperature measured at the active layer of the silicon is assumed to equal the surface temperature [7]. Multiple junction temperature measurements allow for the estimation of the heat transfer coefficient at different regions of the spray, but it is not possible to obtain a detailed surface map of the heat transfer coefficient using this method.

Conventional methods are limited when data from the heat transfer surface with higher spatial resolution is desired. Researchers at the University of Maryland use a dense array of individually controlled heaters. Each of the 96 heaters in the array is 700×700 μm^2 and is controlled by a Wheatstone bridge [1]. The individual heating elements allow for temperature and power measurements at a fairly high spatial resolution with an uncertainty of 5%. As an added benefit, these heaters may be operated in constant heat flux or constant temperature modes, allowing these researchers to study the behavior of boiling and spray impingement past the peak heat flux temperature difference.

Thermochromic liquid crystals (TLC's) have also been used to obtain high resolution measurements of temperatures. By measuring the color or the hue of the TLC's, an estimate of their temperature can be calculated. The application of this measurement technique for mapping heat transfer coefficients is well described by Stasiek [8] and Bayazit et al. [9]. Dano et al. [10] investigated the local heat transfer coefficients under an array of air jets with crossflow on an area of 49 cm^2 using a CCD camera with 640×480 pixel resolution and a transparent orifice plate to view the impingement surface. They report local heat transfer coefficients of a center section of the array with peak values of 800 W m^{-2} K^{-1} and average Nusselt numbers with an uncertainty of 4%. Schmidt and Boye [11] derived heat transfer characteristics of high-temperature spray cooling on a thin electrically heated metal sheet with IR thermography. Average heat transfer coefficients are reported for various flow parameters and temperatures with an uncertainty of the calibrated measurement setup of 6%.

Thus, heat transfer coefficients of spray cooling and other high heat flux systems have been measured with high resolution and accuracy. Unfortunately, these methods are challenging to implement since, in order to obtain truly local heat transfer coefficients, the surface heat flux and local fluid temperature must be known exactly. The TLC method is limited to a fairly narrow range of surface temperatures and also requires careful control of lighting conditions and extensive image processing to extract temperature data from the color information and must be carefully calibrated [12].

1.2. Temperature oscillation IR thermography

Multiple nozzle arrays are required when large surface areas are to be cooled using sprays [13]. Previously reported visualization of multiple nozzle arrays has shown that the resulting fluid flow behavior is very complex [14]. When nozzles in close proximity generate a conical spray, droplets will collide and interfere between adjacent nozzles causing a flow stagnation zone. In this zone, the velocity of the liquid is significantly reduced, resulting in lower heat transfer coefficients and higher surface temperatures, even though the

rate of fluid delivery is higher. Larger surfaces require more nozzles, which in turn leads to more complex draining and more local stagnation regions. To better design nozzle arrays and draining systems, a full surface map of the local heat transfer coefficients is desired. With this information, systems can be designed to achieve more uniform cooling across the active surface and each device on a multi-chip module (MCM) or other large area can be assured of equal cooling. A novel method that can be used to produce a high resolution map of the heat transfer coefficient is temperature oscillation IR thermography (TOIRT).

The TOIRT method was developed for measuring local heat transfer coefficients on heat exchanger surfaces by Wandelt and Roetzel [15] and refined by Freund and Kabalec [16]; it is similar in concept to methods used for measuring the thermal conductivity of materials. The TOIRT method is non-contact, fluid independent and has advantages over other methods, such as the use of TLCs with thin film heaters, that include simplicity of the measurement setup, speed and the absence of any calibration. The TOIRT method relies on the measurement of the temperature response of the outside surface of a heat-transferring wall to an oscillating heat flux. The temperatures of the outer surface are measured with an IR camera and the oscillating heat flux is generated by photon absorption, in this instance from a modulated diode laser. The heat transfer coefficients are derived from the phase delay of the temperature oscillation using a 3-D finite difference thermal model of the wall. The TOIRT method has been previously validated [16] and applied for measurement of local heat transfer coefficients in turbulent pipe flow, for impinging jets of air, for aerodynamic vortex generators in a wind tunnel [17] and on a plate heat exchanger [18]. The method is especially well suited for visualizing heat transfer coefficients with high spatial resolution on flat heat transfer surfaces. As described below, the TOIRT method does not rely on measurements of the applied heat flux or the fluid temperature; it is based only on the temperature response to changes in the heat flux at the surface. Further, it does not require knowledge of the fluid properties.

In this study, the TOIRT method of measuring local heat transfer coefficients was used to characterize two spray cooling designs. A $1.5 \times 1.5\ \mathrm{cm}^2$ area was investigated, and local values for the heat transfer coefficient were found with a resolution of 0.4 mm. The results are compared to a previous experiment that used the conventional method to measure the heat transfer coefficients for the same nozzles at the same flow rates with a thermal die.

2. Experimental approach

2.1. Fluid delivery

The spray cooling system considered in this study is commercially used for spray cooling of multi-chip modules (MCM) in the CRAY X1 (formally known as the SV2) supercomputer, with desired junction temperatures of 70 to 85 °C for heat fluxes from 15 to $55\ \mathrm{W\,cm^{-2}}$ with a Fluorinert™ coolant. Details of the system are described by Pautsch and Bar-Cohen [13] as well as by Pautsch [19].

Fig. 1 displays a schematic of the experimental setup, with the spray cooling module in the center, the heat source and the camera above, and support devices in the periphery. The IR camera used is a FLIR ThermaCAM SC500 that records 30 frames per second with a 320 × 240 resolution. The heat source is a fiber-coupled diode laser with 12 W peak optical power at 685 nm, square wave modulated at a frequency of 0.25 Hz. The laser spot size on the

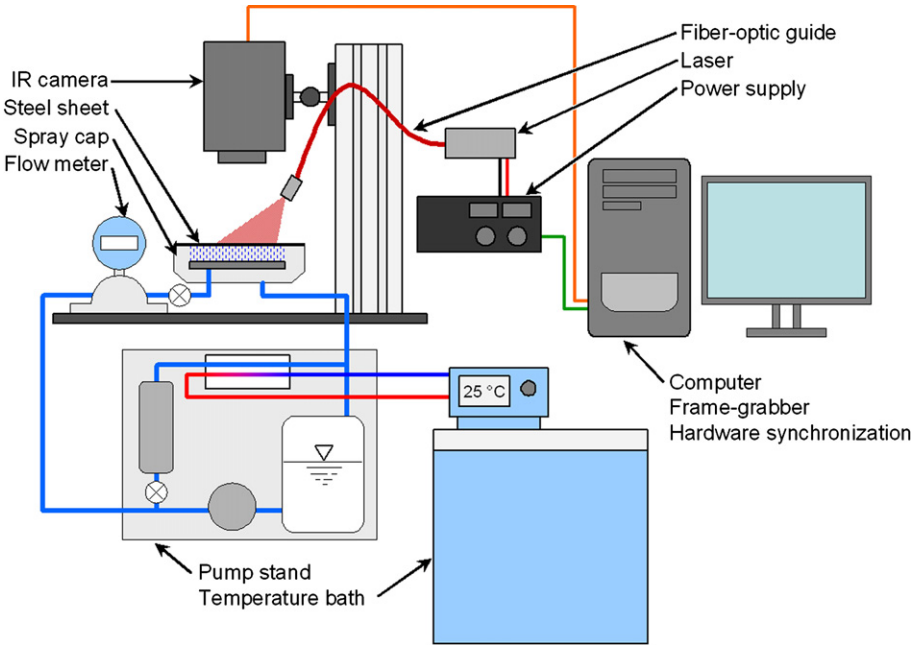

Fig. 1. Schematic of the experimental setup.

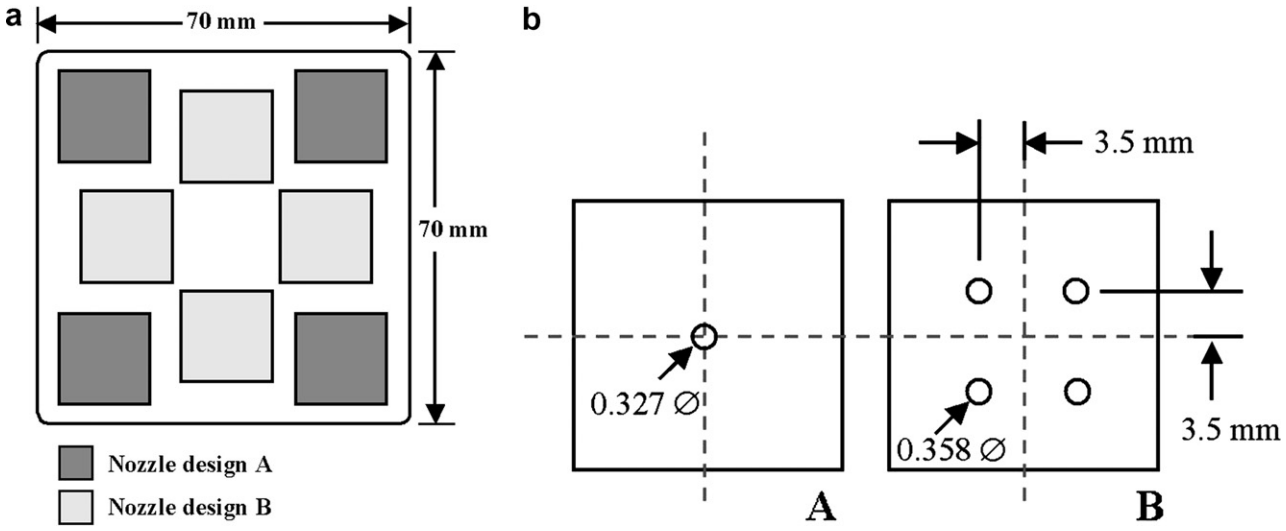

Fig. 2. Relative locations of the nozzle arrays and nozzle geometry.

surface is varied according to the size of the evaluated area; the time averaged heat flux is approximately 1.5 W cm^{-2}. A PC with an IRFlashLink® PCI card and IRLockIn® software records the frames and controls the laser via a programmable Sorenson DC current source. The heat transfer surface was made of ASTM 316 stainless steel coated with black paint ($\epsilon = 0.95$) on the outside for better absorption (total wall thickness 0.272 mm). A variable speed magnetically coupled Idex Corporation MicroPump gear pump is used to deliver the fluid. A needle valve is used to adjust the amount of flow delivered to the nozzles. The volumetric flow rate and fluid inlet temperature are measured with a Krohne Optimass 3050 C coriolis flowmeter. The measurements were taken at three different total flow rates of 0.667, 1.00, and 1.50 min^{-1}, held to within 1%. The fluid inlet temperature was maintained at 25 °C by a thermostatic circulating water bath and a FlatPlate Inc. liquid-to-liquid heat exchanger. The fluid is subcooled and no boiling or significant evaporation occurs at the level of heat flux that was applied.

The spray nozzle plate used for testing contains eight sets of nozzles designed to cool the MCM. As shown in Fig. 2, there are four four-nozzle arrays (design B) and four single-nozzle arrays (design A) that have been described in detail by Pautsch and Shedd [7]. The nozzles spray vertically upwards directly onto the stainless steel plate with a spacing of 5 mm between the nozzles and the heated plate. Nozzle design A is an array of four nozzles cooling a single die, while nozzle design B is a single nozzle. The area of coverage for each nozzle set is designed to be 15 × 15 mm^2. The drain of the cap is located beneath the center of the MCM. Fig. 2 also shows the relative location and size of the nozzles with respect to the area that it is covering.

2.2. Heat transfer measurement

Temperature oscillation methods can derive the heat transfer coefficients from the surface temperature response of a wall heated by a periodic heat flux. The phase delay of the measured temperatures is compared to the solution for the temperature response of a mathematical model of that wall. This is an ill-posed heat conduction problem that must be solved iteratively. Since the state of the system is steady-periodic (after all transient effects have vanished), the system can be treated with harmonic analysis in the frequency domain rather than in the time domain. For the computation of the heat transfer coefficient, only the measured phase delay and the material properties of the wall (thickness, density, thermal capacity and conductivity) are needed. The amplitude of the surface temperature change and the applied heat flux are not needed, so no calibration is required. During the measurement, a periodically modulated laser heats the wall surface and the temperatures are recorded with an IR camera for several oscillation periods after a steady periodic state condition is achieved.

The only heat being supplied to the system is through the radiation from the laser. A 12 W laser was used in this study. The spot size was focused down to the approximate size of the field of view. Two field of view sizes were chosen for testing: 4.7 × 7.0 or 2.1 × 3.2 cm, corresponding to 0.20 and 1.5 W cm^{-2}. The magnitude of the temperature oscillation varied because of the variation in the applied heat and the convection, but magnitudes ranged from 1 to 4 °C peak-to-peak. Because the laser radiation diverges from the source, there is a Gaussian distribution of heat applied to the surface. However, this does not effect the heat transfer measurements because the algorithm used to calculate the heat transfer coefficient is based on a phase delay in the cooling, not the magnitude of the temperature. In addition, all of the applied heat fluxes are within the so-called single-phase spray cooling regime, so no heat flux-dependent heat transfer behavior is expected. Lateral conduction through the 272 μm stainless steel plate is minimal but is accounted for in the numerical model.

The post-processing of the recorded temperature data includes three steps: drift compensation, phase synchronization and Fourier transformation. The drift compensation removes any trend of the temperatures that may be caused by non-steady measurement conditions; de-trending is necessary for the Fourier transformation. To compensate for the drift in temperature between periods, the average temperature over all periods is calculated. Then, the average temperature of each individual period is calculated. The drift is defined as the difference in the average temperature of the last period and the first period divided by the number of periods. If a temperature drift is found, then a compensation in the temperature of each pixel is made by a linear interpolation of the drift from the average temperature such that the first period and the last period have the greatest compensation and the center period has no compensation [16]. To calculate the phase delay of the temperature relative to the heat flux, the timing of the applied heat flux relative to the recorded temperature data must be known exactly. A hardware-independent synchronization procedure is implemented that derives the applied heat flux phase from the temperature data by locating the temperature discontinuity extrema caused by the square wave modulation [17]. Square waves are specifically used to cause these discontinuities in the data to aid in the post processing; the type of waveform is not important for the harmonic response of the real system or the model. The square wave phase synchronization proved to be more reliable than previous attempts of synchronizing the heat flux modulation to the IR frame recording on the hardware side. The temperature phase delay is calculated with single frequency discrete Fourier transformations (SFDFT) for each pixel over every frame. The SFDFTs yield the matrix of the phase delay $\phi(x,y)$, which is rescaled and used as the input of the numerical model for the computation of the heat transfer coefficients $h(x,y)$.

The model is a 3-D complex finite difference model that was validated by comparison to an analytical solution from Wandelt and Roetzel [15] and to FEM calculations in ANSYS®. The model assumes a thermal input on one side due to radiation and neglects any cooling due to free convection. This is an acceptable assumption because the temperature of the irradiated surface never rises above the ambient (since the liquid is colder than the ambient). In addition, the magnitude of the heat transfer coefficient on the back side of the plate is far greater in magnitude and the bulk of the thermal energy will penetrate through the metal. Details of the model and the validation, as well as a consideration of potential errors at steep gradients caused by the ill-posed nature of the problem, can be found in Freund and Kabelac [16]. The model is solved iteratively with a sparse matrix algorithm in order to yield a matrix of the heat transfer coefficients $h(x,y)$ for the input matrix of the measured phase delay $\phi(x,y)$. All data processing and calculations are performed in Matlab®.

Experiments were performed where the entire spray cap was imaged, as well as experiments concentrating on a single nozzle and a four nozzle array. Because a fixed-focus optical system was utilized, the field of view was constrained by the available lenses. After the numerical model was run to calculate the local heat transfer coefficients, the resulting data arrays were cropped to rectangular regions representing the areas that the nozzle sets were designed to cool. The cropping also eliminates noise at the edges of the data arrays due to numerical edge effects.

The following analysis considers the accuracy of the computed heat transfer coefficients based on the uncertainty of the measured phase delay and the heat transfer wall parameters. For this analysis, the wall parameters, the heat transfer coefficient and the frequency are combined into two dimensionless groups according to Wandelt and Roetzel [15] using the thermal diffusivity α, the thermal conductivity k, the wall thickness δ and the angular frequency ω: the non-dimensional heat transfer coefficient

$$\psi = \frac{h\alpha}{k\delta\omega} \tag{2}$$

and the dimensionless thickness

$$\xi = \frac{\text{wall thickness}}{\text{thermal penetration depth}} = \delta\sqrt{\frac{\omega}{2\alpha}} \tag{3}$$

These non-dimensional variables allow for the coverage of nearly all possible experimental parameters with just two variables.

2.3. Spatial resolution

An estimate for the limit of spatial resolution follows directly from the definition of ξ in Eq. (3). If $\xi < 0.5$, then the lateral diffusion of thermal energy is essentially negligible compared with the rate of diffusion through the wall. For this experiment, $\alpha = 3.48 \times 10^{-6}\,\mathrm{m^2\,s^{-1}}$, $\omega = \pi/2\,\mathrm{s^{-1}}$ and $\delta = 272\,\mu\mathrm{m}$, giving $\xi = 0.129$. Thus, the spatial resolution is expected to be limited by the resolution of the camera and not by lateral diffusion.

2.4. Uncertainty in heat transfer measurements

Fig. 3 shows the phase delay ϕ as a function of these dimensionless parameters, derived using a one-dimensional analytic solution. The accuracy of the calculated heat transfer coefficient h relies on the accuracy of the measured phase delay ϕ as well as the wall parameters δ, ρ, and c, when an exact solution for $h(\phi)$ is provided. Fig. 3 shows that the rate of change of the phase delay with respect to the heat transfer coefficient, the inverse sensitivity, depends on ψ. The minimum relative error $\Delta h/h$ corresponding to a measurement error $\Delta\phi$ is expected where the sensitivity is lowest, i.e., where the gradient in Fig. 3 is steepest. Thus, the oscillation frequency should be chosen to yield a ψ on the order of unity and a $\xi < 1$. Measurements with either very low or high ψ or a ξ approaching $\pi/2$ will fail, since the sensitivity to input inaccuracies is too high.

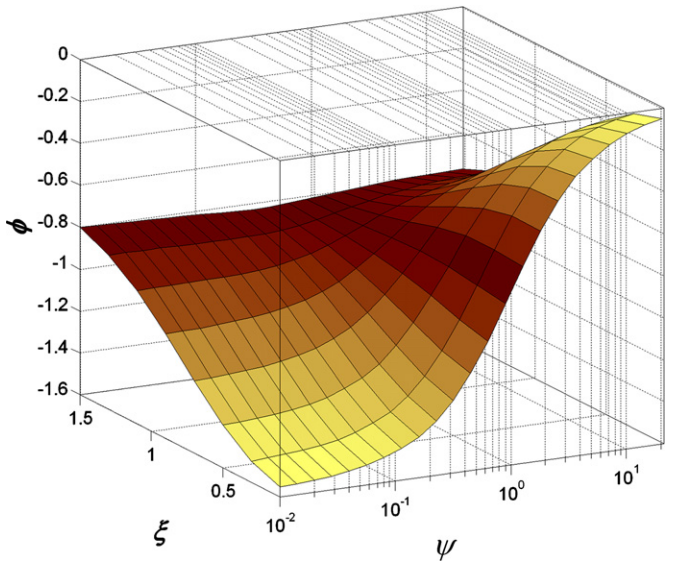

Fig. 3. Temperature phase delay ϕ as a function of the dimensionless parameters ξ and ψ.

The error of the measured phase delay is sensitive to two factors, the signal-noise ratio and the phase synchronization between heat flux and temperature oscillation. The signal-noise ratio is defined here as the temperature oscillation amplitude divided by the standard deviation of the zero-mean fluctuation of the IR camera's detector. Generally, the signal-noise ratio (SNR) in these measurements is quite low, and it is only due to the averaging of hundreds of temperature values within the Fourier transformations that useful data can be derived. The phase delay error RMS is inversely proportional to both the SNR and the square root of the number of frames. For a measurement with a frequency of 0.25 Hz and 30 frames per second over five periods, the RMS of the phase delay error is 0.0144 at an SNR of 4. A generalized empirical formula for the local phase error is given in Eq. 4, with i as the number of frames:

$$\Delta\phi(\mathrm{SNR},i) = \frac{\sqrt{2}}{\mathrm{SNR}\sqrt{i}} \tag{4}$$

The error $\Delta\phi$ is the local uncertainty of the phase delay values. Area averaged phase delay values are much less affected by the noise, as the error decreases with the square root of the number of averaged values. Usually, the phase values of at least four pixels are averaged before calculating the heat transfer coefficients, reducing the noise-induced errors by a factor of at least two. The error in the phase synchronization arises from any inaccuracy in the relation of the heat flux and the frame timing. When the hardware independent square wave phase synchronization is used, the phase error again depends on the SNR and the number of evaluated periods. For low SNR, the errors of the phase synchronization increases and more periods should be evaluated to gain a better average of the phase angles of the extrema. Typically, the standard deviation of the extrema phase angle is less than half of the time delay between frames. Thus, a maximum phase synchronization error of 1/2 of the frame time step is assumed, which is 0.0262 rad at 30 frames per second. For local phase values $\phi(x,y)$, the sum of both errors must be considered, while for average values, the synchronization error dominates. Table 1 shows the results of an uncertainty propagation of the input errors through the calculation of the heat transfer coefficients using the 1-D analytical solution from Wandelt and Roetzel [15], assuming an uncertainty of 5% in the material properties and ±2.5 μm in the wall thickness.

Table 1
Uncertainty propagation for single measurements

$\overline{h_m}$ (W cm^{-2} K^{-1})	$\Delta h/h$		SNR
	Local (%)	Average (%)	
0.4	10.8	6.6	4
0.8	20.8	14.0	2

The values summarized in Table 1 are the maximum expected errors associated with a single measurement. The results presented here are each an average of four single measurements, effectively reducing the errors by a factor of two; therefore we state the uncertainties for the average values as $< 5\%$ and for local values, depending on the magnitude, between 5% and 10%.

3. Results

Measured heat transfer coefficients are presented here for the whole MCM cooling module as well as for the four-nozzle array and the single nozzle individually, enlarged to show measurements that are more detailed. The liquid flowrates through the entire nozzle array (20 nozzles) are 0.67, 1.0 and 1.5 min^{-1}, respectively, with a corresponding pressure drop through the nozzles of 69.0, 138, and 310 kPa. The droplet flux rates of the individual nozzles or nozzle arrays are estimated based on the design conditions from the manufacturer and are divided by the area to be cooled. The actual measurement data and the numerical model consider an area larger than the shown results in order to prevent numerical edge effects from the model.

3.1. Full nozzle array

Fig. 4a–c illustrates maps of the heat transfer coefficients measured on a 60 × 44 mm^2 section of the plate with a resolution of 0.8 mm^2 for the three flowrates. The entire spray coverage area shown in Fig. 2 could not be captured in the camera field of view; the upper two single-nozzle arrays are not visible, as well as half of the upper four-nozzle array. The figures show areas of high heat removal above the spray nozzles and low heat transfer coefficients between them. The peak values increase from 1.2 to 2.0 W cm^{-2} K^{-1}. The heat transfer coefficient surrounding the nozzles is remarkably uneven, with some nozzles performing significantly worse than others. The performance is affected by both the nozzle spray patterns and the local

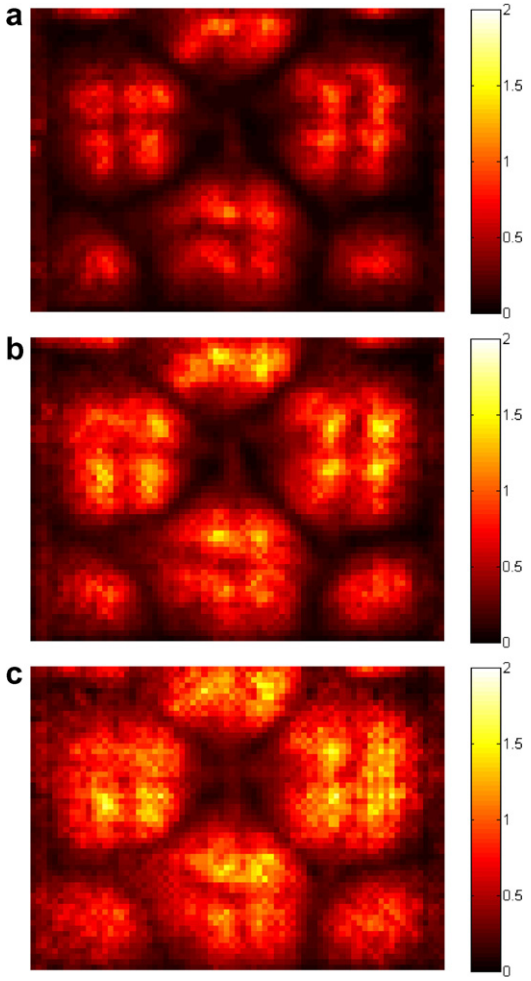

Fig. 4. Heat transfer coefficients in W cm^{-2} K^{-1} on MCM for (a) 0.67, (b) 1.0 and (c) 1.5 l min^{-1}.

fluid flow, making uniform draining an important issue. These wide field of view images are intended to show the variation between the nozzle arrays due to spray distribution and liquid interaction on the surface.

3.2. Four nozzle array

In Fig. 5a–c, the heat transfer coefficients on a 1.5 × 1.5 cm^2 area above a four-nozzle array (nozzle design B) are shown with a resolution of 0.4 mm^2 for droplet fluxes of (a) 1.00, (b) 1.50 and (c) 2.25 ml s^{-1} cm^{-2}. The peak values increase from 1.3 to 2.0 W cm^{-2} K^{-1} as flow increases. The heat transfer coefficients associated with the upper left nozzle were lower than for the other nozzles, apparently due to nozzle imperfections, which will be discussed further below.

3.3. Single nozzle

The heat transfer coefficients on a 1.5 × 1.5 cm^2 area above a single nozzle (nozzle design A) are shown in Fig. 6a–c for flow rates of (a) 0.234, (b) 0.352 and (c) 0.528 ml s^{-1} cm^{-2} with a resolution of 0.4 mm. The peak values directly above the nozzle increase from 1 to 1.5 W cm^{-2} K^{-1} as flow increases. The heat removal is high directly above the spray, but as the fluid moves out radially along the surface, the momentum of the fluid is lost and the heat transfer coefficient decreases. This pattern matches the results obtained by Pautsch [7], who found the highest performance of this nozzle design to be at the center with the lowest performance at the corners. Circumferentially averaged heat transfer coefficients as a function of the radial distance from the single nozzle are plotted in Fig. 7.

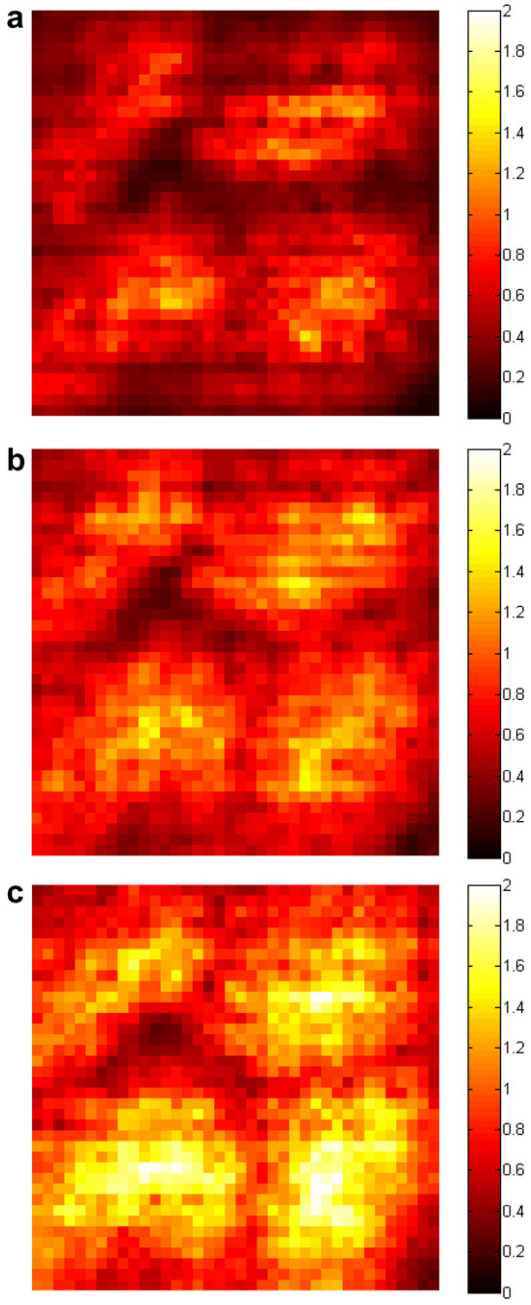

Fig. 5. Heat transfer coefficients above a four-nozzle array in W cm^{-2} K^{-1} for (a) 1.00, (b) 1.50, and (c) 2.25 ml s^{-1} cm^{-2}.

As noted above, Horacek et al. used an array of 0.7 × 0.7 mm^2 heaters to obtain information on local spray

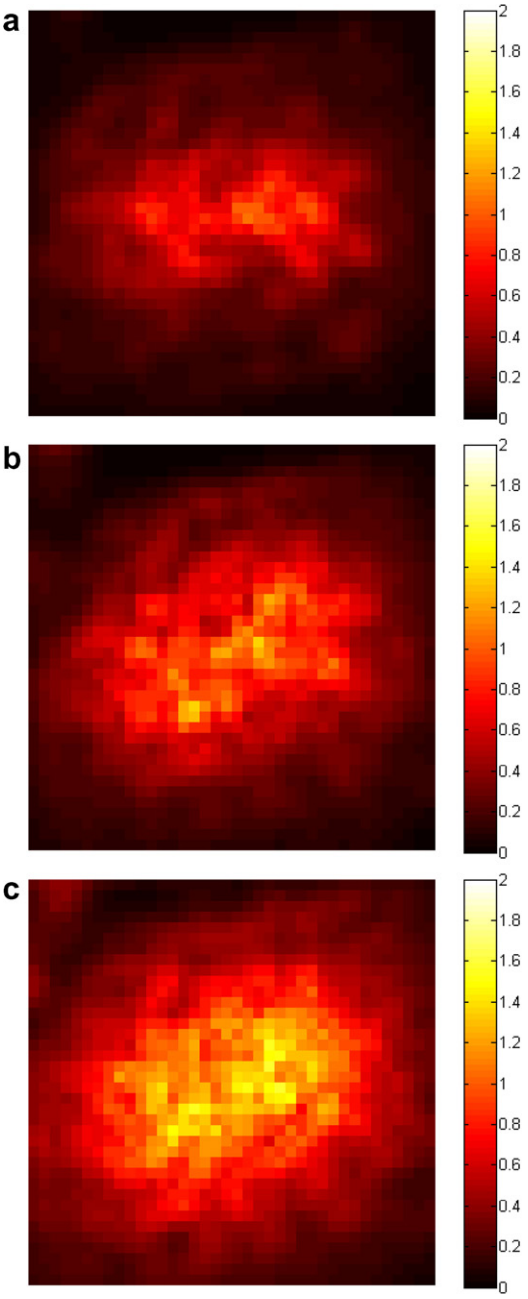

Fig. 6. Heat transfer coefficients above single nozzle in W cm^{-2} K^{-1} for (a) 0.234, (b) 0.352, and (c) 0.528 ml s^{-1} cm^{-2}.

heat transfer behavior. Although they do not present heat transfer coefficient data, they may be inferred from Fig. 6 of Ref. [20] and the spatial trends in their data correspond closely to those presented here.

3.4. Spatially averaged results

The heat transfer coefficients for the single- and four-nozzle arrays averaged over the cooling area of 1.5 × 1.5 cm^2 are listed in Table 2. The area-averaged values indicate an almost linear increase of the heat transfer coefficients with the flowrate. The comparison of the two arrays shows that the four-nozzle array has about twice

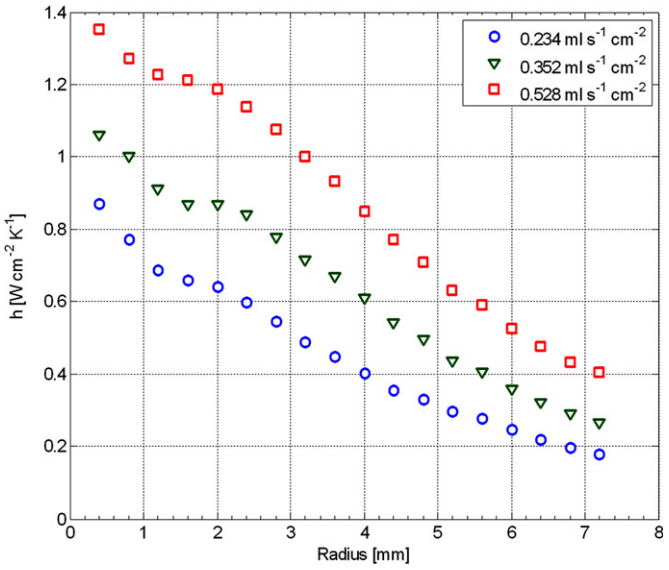

Fig. 7. Heat transfer coefficients over the radial distance from a single spray nozzle.

Table 2
Average heat transfer coefficients for a 1.5 × 1.5 cm^2 area for the single- and four-nozzle array and comparison of the TOIRT method with prior data derived with the conventional method for similar flow rates and applied heat fluxes

Flow rate (ml s^{-1} cm^{-2})	TOIRT method (W cm^{-2} K^{-1})	Conventional method (W cm^{-2} K^{-1})
Single-nozzle array		
0.234	0.25	0.20
0.352	0.37	0.30
0.528	0.54	0.45
Four-nozzle array		
1.000	0.55	0.60
1.500	0.76	0.80
2.250	1.02	1.10

the performance of the single nozzle but at four times the flow rate.

The current heat transfer coefficient measurements taken with the TOIRT method are in Table 2 also compared to measurements taken with the conventional method. In that previous experiment, thermal test dies with eight embedded temperature sensing diodes were used to obtain an average heat transfer coefficient with varying flow rates and heat fluxes [7]. For these data, the values of $\overline{h_m}$ are an estimate based on the lowest applied heat flux, since the heat transfer coefficient becomes heat flux dependent at high heat fluxes [7] and the TOIRT method used a low power heat source.

Table 2 shows agreement in the measurements of the heat transfer coefficients between the conventional and the TOIRT method of 25% or better for the single nozzle and within 10% for the four-nozzle array. For the multiple nozzle array, the TOIRT values are always slightly lower than the values from prior measurements. This is likely

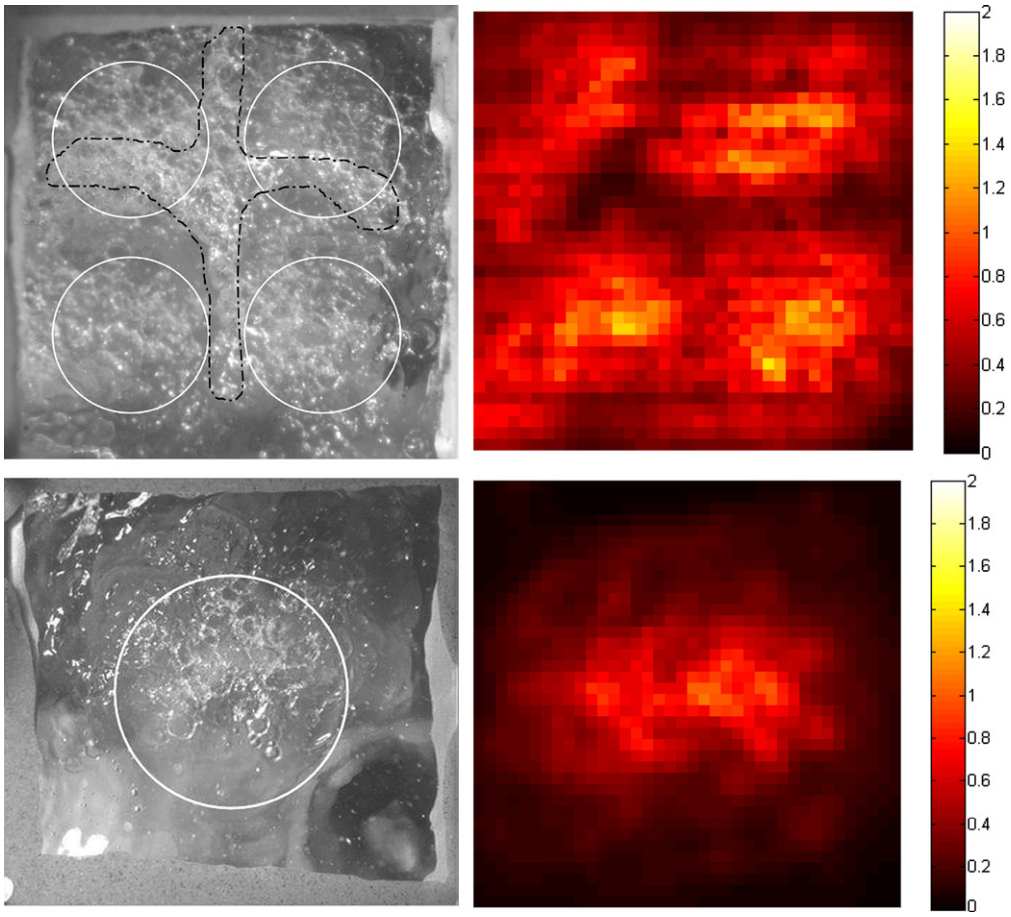

Fig. 8. Visualization of a typical (top) four-nozzle array and (bottom) single nozzle and the measured heat transfer coefficients.

because the TOIRT method is able to measure the values of heat transfer coefficient in the interference regions of the die, where they are at their lowest. Since there were no thermal diodes located in the spray interference region on the MCM thermal test dies, the conventional method does not include those lower-performing regions in its average. For the single nozzles, the TOIRT method found higher heat transfer values than the prior measurements with the conventional method. An explanation for this is that the previous measurement was more heavily averaged to the outside of the die where most of the thermal diodes were located: only one value was measured at the center, the other values were measured at the edge or outside the spray region, leading to a lower reported heat transfer coefficient.

3.5. Comparison with visualization

In a previous study, it was theorized that the heat transfer performance of multi-nozzle arrays in spray cooling systems can be correlated by three terms accounting for sensible heating of the liquid beneath the spray impingement area, latent heat of vaporization due to evaporation from the liquid film surface, and sensible heating of liquid draining between nozzles [14]. Visualization of the nozzles spraying onto a transparent surface gives support for this theory. Pautsch and Shedd identified two important regions in the four nozzle arrays tested, the spray impact region and the spray interaction/draining region [21], and they theorized that the heat transfer performance is vastly different between these two regions due to a loss of fluid momentum when droplets from neighboring nozzles collide. The results of the TOIRT experiment further support this theory. The left of Fig. 8 shows a four-nozzle array spraying onto a transparent surface, while the right is a map of the heat transfer coefficient for a similar nozzle design. On the left, the white circles represent the approximate areas where the spray directly impacts the film. The dark dashed line traces a region of high turbulence and vapor entrainment that is believed to be associated with nozzle interactions and draining. Characterization of the nozzles from the manufacturer has shown a 5 to 10 % variation in nozzle flow rates due to manufacturing tolerances. A clear correlation can be seen between the turbulent interaction region and the areas of lower heat transfer coefficients.

4. Summary

Spray cooling systems offer great potential for high heat flux applications such as next generation computer chips or

power electronics, e.g., IGBTs, due to high heat transfer coefficients. With the TOIRT method described here, locally resolved measurements can be obtained with high accuracy and resolution. The results show local peak values of $2.0\,W\,cm^{-2}\,K^{-1}$ and average values of up to $0.54\,W\,cm^{-2}\,K^{-1}$ for a single nozzle and $1.0\,W\,cm^{-2}\,K^{-1}$ for a four-nozzle array on an area of $1.5 \times 1.5\,cm^2$. These values match the heat transfer coefficients measured with the same nozzles at equivalent flow rates using conventional method within 25% and 10%, respectively.

Significant maldistribution of heat transfer performance occurs, with some nozzles performing almost two times lower than others, exacerbated by the influence of the local liquid film flow caused by uneven draining. This uncertainty of performance limits the minimum safety margin for maintaining maximum junction temperatures on chips. This new technique provides a tool for improving the uniformity of heat transfer performance in spray cooling and other high heat flux removal systems, thus improving overall system performance and reliability.

At this time, the level of heat that can be delivered to the system is limited by the power of the laser used as the radiation source. With the current level of heat, no evaporation of fluid is expected. To be able to measure the heat transfer coefficient in different regimes of spray cooling, heat loads larger than the ones tested in this report are required. For example, an additional source of radiation could be applied continuously while the primary laser is oscillated. Otherwise, the technique described here could be implemented without change.

Acknowledgements

The authors appreciate funding granted by Cray, Inc. to the Multiphase Flow Analysis and Visualization Laboratory at the University of Wisconsin–Madison through the Defense Advance Research Projects Agency High Performance Computing program and by the German Research Council (DFG) for the project "Heat Transfer on Complex Flows" at the University of the Federal Armed Forces in Hamburg. The authors are grateful to the Wisconsin Electric Machines and Power Electronics Consortium for the use of their IR camera.

References

[1] B. Horacek, K.T. Kiger, J. Kim, Single nozzle spray cooling heat transfer mechanisms, Int. J. Heat Mass Transfer 48 (2005) 1425–1438.
[2] I. Mudawar, K.A. Estes, Optimizing and predicting CHF in spray cooling of a square surface, J. Heat Transfer 118 (1996) 672–679.
[3] L. Lin, R. Ponnappan, Heat transfer characteristics of spray cooling in a closed loop, Int. J. Heat Mass Transfer 46 (20) (2003) 3737–3746, September.
[4] A.C. Cotler, E.R. Brown, V. Dhir, M.C. Shaw, Chip level spray cooling of an LD-MOSFET RF power amplifier, IEEE CPT Trans. 27 (2004) 411–416.
[5] G. Croce, H. Beaugendre, W.G. Habashi, Numerical simulation of heat transfer in mist flow, Numer. Heat Transfer Part A 42 (2002) 139–152.
[6] C. Lee, K. Lee, J. Senda, H.A. Fujimoto, study on the spray wall interaction model considering degree of superheat in the wall surface, Numer. Heat Transfer Part B: Fundamentals 40 (6) (2001) 495–513.
[7] A.G. Pautsch, T.A. Shedd, Spray impingement cooling with single- and multiple-nozzle arrays Part I: Heat transfer data using FC-72, Int. J. Heat Mass Transfer 48 (2005) 3167–3175.
[8] J. Stasiek, Thermochromic liquid crystals and true colour image processing in heat transfer and fluid-flow research, Heat Mass Transfer 33 (1997) 27–39.
[9] B.B. Bayazit, D.K. Hollingsworth, L.C. Witte, Heat transfer enhancement caused by sliding bubbles, J. Heat Transfer 125 (3) (2003) 503–509, June.
[10] P.E. Dano, J.A. Liburdy, K. Kanokjaruvijit, Flow characteristics and heat transfer performance of a semi-confined array of jets: effect of nozzle geometry, Int. J. Heat Mass Transfer 48 (2005) 691–701.
[11] J. Schmidt, H. Boye, Influence of velocity and size of the droplets on the heat transfer in spray cooling, Chem. Eng. Technol. 24 (2001) 255–260.
[12] D.J. Farina, J.M. Hacker, R.J. Moffat, J.K. Eaton, Illuminant invariant calibration of thermochromic liquid crystals, in: R.J. Simoneau, B.F. Armaly (Eds.), Visualization of Heat Transfer Processes, vol. HTD–vol. 252 of 29th National Heat Transfer Conference, Atlanta, GA, August, ASME, 1993, pp. 1–11.
[13] G. Pautsch. An overview on the system packaging of the CRAY SV2 supercomputer, in: Proceedings of IPACK'01, The Pacific Rim/ASME International Electronic Packaging Technical Conference and Exhibition, ASME, 2001, pp. 617–624.
[14] T.A. Shedd, A.G. Pautsch, Spray impingement cooling with single- and multiple-nozzle arrays. Part II: Visualization and empirical models, Int. J. Heat Mass Transfer 48 (2005) 3176–3184.
[15] M. Wandelt, W. Roetzel, Lock-in thermography as a measurement technique in heat transfer, Quant. Infrared Thermogr. 96 – Eurotherm Series 50 (1997) 189–194.
[16] S. Freund, S. Kabelac. Measurements of local convective heat transfer coefficients with temperature oscillation IR thermography and radiant heating, in: Proceedings of ASME Summer Heat Transfer Conference, San Francisco, CA, July, 2005.
[17] S. Freund, S. Kabelac, IR measurement of temperature oscillations to investigate convective heat transfer coefficients on heat exchangers, Int. J. Heat Exchang., to appear.
[18] S. Freund, S. Kabelac, Local convection coefficients in plate heat exchangers measured with temperature oscillation IR thermography, in: Proceedings of 13th International Heat Transfer Conference, Sydney, Australia, August, 2006.
[19] A.G. Pautsch, Heat transfer and film thickness characteristics of spray cooling with phase change. Master's thesis, University of Wisconsin–Madison, Madison, Wisconsin, 2004.
[20] B. Horacek, J. Kim, K.T. Kiger. Effects of noncondensable gas and subcooling on the spray cooling of an isothermal surface. In Proceedings of the ASME IMECE 2003, Washington, DC, November, 2003. American Society of Mechanical Engineers. Paper IMECE2003-41680.
[21] A.G. Pautsch, T.A. Shedd, Adiabatic and diabatic measurements of the liquid film thickness during spray cooling with FC-72, Int. J. Heat Mass Transfer 49 (2006) 2610–2618.